Bull Volcanol (2006) 68: 294–307
DOI 10.1007/s00445-005-0008-7

RESEARCH ARTICLE

Alicé S. Davis · David A. Clague

Volcaniclastic deposits from the North Arch volcanic field, Hawaii: explosive fragmentation of alkalic lava at abyssal depths

Received: 23 September 2003 / Accepted: 2 May 2005 / Published online: 18 October 2005

Abstract Submarine explosive eruptions are generally considered to become less likely with increasing depth due to the increasing hydrostatic pressure of the overlying water column. Volcaniclastic deposits from the North Arch volcanic field, north of Oahu, have textural characteristics of explosive fragmentation yet were erupted in water depths greater than 4,200 m.

The most abundant volcaniclastic samples from North Arch are clast-supported with highly vesicular, angular pyroclasts. They are most likely near-vent pyroclastic fall deposits formed in eruption columns of limited height. Interbedded with highly vesicular pillow lava, they form low (50 to 200 m), steep-sided cones around the vents. Less common are stratified samples with graded bedding; one such sample includes a layer of roughly aligned, platy, bubble-wall glass fragments (resembling littoral limu o Pele) that may have been deposited by density currents. In addition to bubble-wall glass shards, numerous glass fragments with spherical, delicate spindle and ribbon shapes, and Pele's hair-like glass strands occur in the finer size fraction (<0.5 mm) of some samples. They are probably more distal fallout. Another sample, consisting of glass fragments dispersed in a marine clay matrix, was apparently reworked and deposited farther from the vents by bottom currents.

Glass compositions include low-(~0.4-0.6 wt%) and medium-K_2O (>0.6 wt%) alkalic basalt, basanite, and nephelinite. Sulfur and chlorine abundances are high, reaching a maximum of 1,800 and 1,300 ppm, respectively. The ubiquitous presence of limu o Pele fragments, regardless of glass composition, suggests that bursts of Strombolian-like activity accompanied most eruptions. Coalescing vesicles observed in larger pyroclasts and some pillow lava suggests accumulation of volatiles. Since the great hydrostatic pressure makes steam expansion impossible, a volatile-rich, supercritical magmatic fluid probably drove the eruptions. If these volatile-rich magmas had erupted in shallow water or subaerially, tall fountains would most likely have resulted. The great hydrostatic pressure (>40 MPa) limited fountain and eruption column heights.

Keywords Submarine explosions · Strombolian · Pyroclastic fragmentation · Lava bubble wall fragments · Alkalic basalt · North Arch volcanic field · Hawaii

Editorial responsibility: J. McPhie

A. S. Davis (✉) · D. A. Clague
Monterey Bay Aquarium Research Institute,
7700 Sandholdt Road, Moss Landing, CA, 95039-9644, USA
e-mail: davisa@mbari.org
Tel.: +831-775-1857

Introduction

Volcaniclastic deposits include all clastic volcanic material formed by a range of fragmentation processes and dispersed and deposited in any environment (Fisher 1961). Explosive fragmentation may occur due to (1) decompression and expansion of volatile constituents dissolved in magma, (2) disruption of lava by steam expansion, or (3) shattering of pre-existing volcanic rock due to steam expansion. Fragmentation can also be non-explosive due to cooling granulation as hot lava is quenched in cold water. Fragmentation of magma due to decompression and expansion of dissolved volatile elements as magma rises and erupts has been observed for many volcanoes on land. Explosive subaerial eruptions are commonly classified as strombolian, hawaiian, vulcanian, and plinian (e.g. Fisher and Schmincke 1984). Some disagreement exists with respect to terminology, especially with regard to Strombolian activity (see Parfitt 2004 for a review). In this paper, we use Strombolian activity to refer to small, discrete explosions, in contrast to more continuous fountaining that characterizes Hawaiian activity (Parfitt 2004).

Volcaniclastic deposits formed in marine environments are abundant in the geologic record of many tectonic settings (e.g. Fisher and Schmincke 1984; Cas and Wright 1987, and references therein), testifying to similar processes operating in submarine and subaerial environments.

However, no explosive eruption has ever been observed in the deep sea and interpretation of the formation of marine volcaniclastic deposits rests primarily on comparison with deposits on land and on data derived from experimental studies (e.g. Zimanowski et al. 1997).

Volcanic fragments produced in subaerial Hawaiian fountains are characteristically highly vesicular, ragged, and/or aerodynamically shaped. They may include delicate droplet-, ribbon- and spindle-shapes, or hair-like strands, such as Pele's hair. Welding and agglutination of molten lava fragments (spatter) is especially common in subaerial eruptions. Thin, curved, bubble-wall fragments, called limu o Pele (Hon et al. 1988), have been observed forming when lava flowing into the ocean is stretched by trapped water expanding to steam. Limu o Pele (literally Pele′s seaweed, Hon et al. 1988) is a descriptive term indicating that the particles physically resemble seaweed in being light brown and flat, and larger fragments have shiny corrugated surfaces.

Curved bubble-wall glass shards, closely resembling littoral limu o Pele, have also been described from 1,000–1,900 m depth on the summit and south rift zone of Loihi Seamount (Clague et al. 2003a). Clague et al. (2000) initially attributed their formation to steam expansion. The ubiquitous presence of limu o Pele fragments along the Gorda mid-ocean ridge, erupted at depths exceeding the critical pressure for seawater boiling, led Clague et al. (2003b) to propose that deep-sea limu o Pele particles could also form due to discharge of an accumulated, magmatic volatile phase during mild Strombolian eruptions. The limu o Pele fragments from the Gorda Ridge and those from Loihi Seamount are morphologically identical and Clague et al. (2003a) therefore inferred that both formed by the same process. However, morphologically similar limu o Pele fragments found on seamounts near the East Pacific Rise (Maicher and White 2001) were attributed to steam expansion of water-saturated sediment trapped under lava flows. In each of these studies, the thin, platy, slightly curved, bubble-wall, glass particles were referred to as limu o Pele. We use the term here to describe morphologically similar particles without implying a formational process.

Interpretation of the mechanism(s) of fragmentation is based largely on clast morphology, which is closely related to the mode of magma-water interaction (Wohletz 1983). Aerodynamic fragment shapes and evidence for ductile deformation observed in submarine volcanic fragments are indicative of at least mildly explosive subaqueous eruptions. Welded or agglutinated spatter, however, appears to be absent due to rapid quenching in water. One fundamental difference between subaerial and submarine eruptions is much more efficient quenching in the latter, resulting in formation of ubiquitous basaltic glass.

At pressures greater than 29.8 MPa (equivalent to about 2,940 m depth in the northern Pacific Ocean near Hawaii), the critical point for expansion of seawater to steam (Bischoff and Rosenbauer 1988), explosive eruptions were thought not to be feasible. However, Wohletz (2003) proposed that localized vapor expansion is possible at higher ambient pressure and provided a theoretical model for explosive volcanism to depths exceeding 4,000 m, although it is unclear whether fluidal-shaped particles can be formed by his oscillating supercritical fluid film model.

Volcaniclastic deposits become more abundant on ocean island volcanoes as the volcano grows to shallow water depth (e.g. Staudigel and Schmincke 1984) indicating greater expansion of volatile constituents with decreasing hydrostatic pressure. For low- volatile, tholeiitic basaltic magma, explosive fragmentation was proposed to be limited to water depths of a few hundred meters (e.g. Moore and Schilling 1973). For magmas more enriched in volatiles, explosive fragmentation appears to be possible at much greater depths (e.g. Gill et al. 1990; Clague et al. 1990, 2000, 2002, 2003a; Davis et al. 2002; Davis and Clague 2003; Head and Wilson 2003; Hékinian et al. 2000; Fouquet et al. 1998; Eissen et al. 2003).

Here we describe volcaniclastic deposits from four locations in the North Arch volcanic field. These deposits were erupted at abyssal depths exceeding 4,200 m, yet they have textural features characteristic of explosive fragmentation. The textural and compositional characteristics of the deposits from these sites, where eruption depth is well constrained, provide proof of, and insight into, explosive fragmentation processes under extreme hydrostatic pressure.

Geological setting and previous work

The North Arch volcanic field is located on the deep-sea floor north of Oahu (Fig. 1). The lavas cover an area of about 24,000 km^2 (Clague et al. 2002) at water depths ranging from 3,900 to 4,380 m. Straddling the Hawaiian flexural arch, the Plio-Pleistocene lavas and vent structures have an estimated volume between 1,000 and 1,250 km^3 (Clague et al. 2002). SeaBeam bathymetry of the lava field shows nearly 100 volcanic vents, ranging from low-relief shields to small, steep-sided cones (Clague et al. 2002). Several lava flows, emanating from the base of the cones, extend long distances (>100 km) over nearly flat terrain (~1.5 m/km slope). The Pleistocene lavas surround Cretaceous seamounts and sediment-covered kipukas, which are distinguishable by their different side scan characteristics (Clague et al. 1990).

The lavas from the North Arch volcanic field have been the focus of numerous geochemical studies. Chemical and petrographic data for samples collected with dredges from the North Arch volcanic field and glass chemistry of additional samples collected with the submersible *Shinkai 6500* on a JAMSTEC cruise of the *R/V Yokosuku* in 2000 were reported by Clague et al. (1990, 2002, respectively). Dixon et al. (1997) analyzed glass rinds from many of the dredge samples for volatile constituents, presented detailed degassing models, and calculated initial volatile contents. They observed good agreement between H_2O and CO_2 contents and predicted vapor saturation at 40 MPa, in agreement with an eruption depth of about 4,000 m. Frey et al. (2000) presented trace element, isotopic, and mineralogic compositions of dredged whole-rock samples and

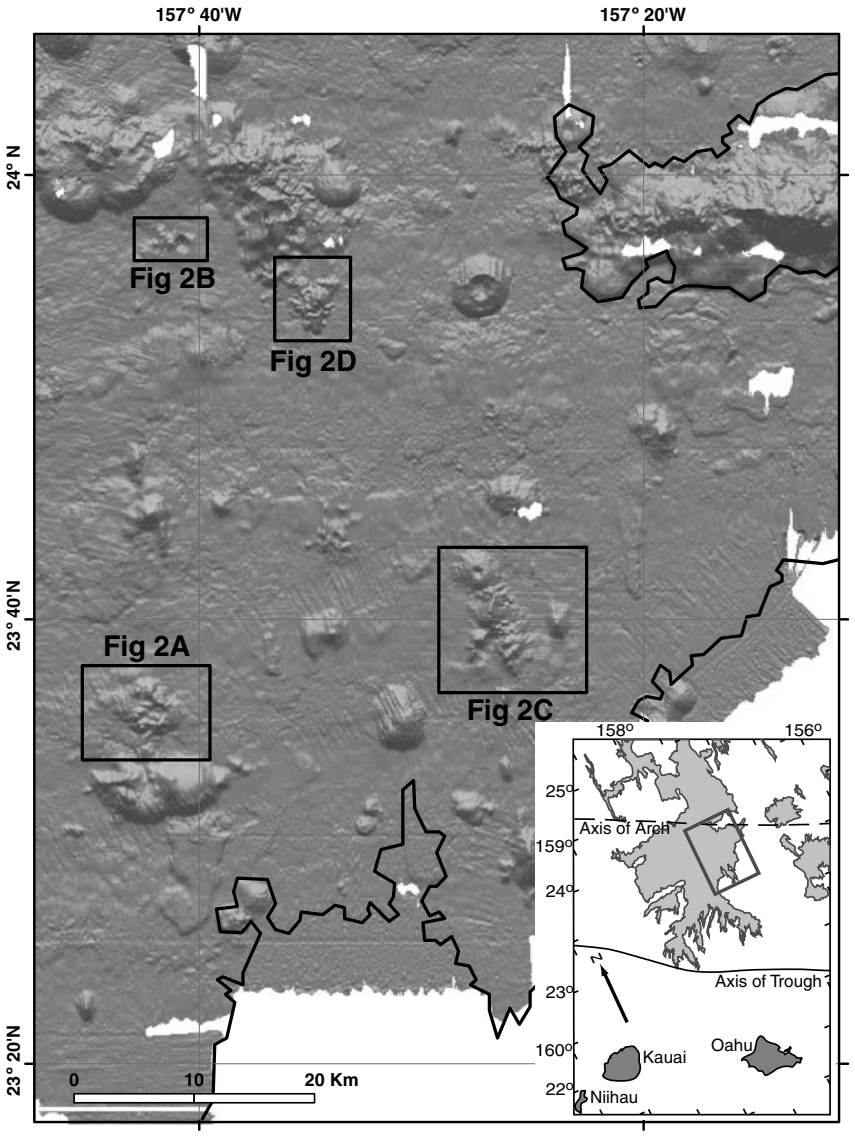

Fig. 1 Shaded relief image of SeaBeam bathymetry map of North Arch volcanic field. *Inset* shows location relative to the Hawaiian Islands. Flow field is based on GLORIA imagery. *Boxes* outline the detailed maps shown in Fig. 2 where volcaniclastic deposits were recovered. The *black line* indicates the margin of the flow field. The *large cratered cone* and ridges along northern margin are Cretaceous in age

evaluated magma genesis for the North Arch lavas. Most recently, Yang et al. (2003) used an internally consistent trace element data set to compare the genesis of the North Arch and Honolulu Volcanics. These studies have established that lavas of the North Arch volcanic field consist of alkalic basalt, basanite, and nephelinite that are compositionally similar to rejuvenated-stage lavas of the Hawaiian Islands, such as the Honolulu (Clague and Frey 1982) and Koloa Volcanics (Clague and Dalrymple 1988; Maaloe et al. 1988; Reiners and Nelson 1998; Reiners et al. 1999). The volatile data (Dixon et al. 1997) are especially important for understanding fragmentation processes that formed the volcaniclastic deposits described here.

Sampling and analytical methods

Samples of volcaniclastic deposits were recovered in dredges 26D and 27D on a U.S. Geological Survey cruise (F11-88HW) of the *R/V Farnella* in 1988 (Clague et al. 1990). Dive samples S502 and S503 were collected with the submersible *Shinkai 6500* in 1999 (Clague et al. 2002). Additional samples of loosely cemented volcaniclastic deposits were recovered on dive S704 of the *Shinkai 6500* in 2002. Polished thin sections were examined with a petrographic microscope and glass analyses were done with a JEOL JX 8900 Superprobe at the U.S. Geological Survey in Menlo Park, using natural and synthetic glass and mineral standards (Davis et al. 1994). An accelerating voltage of 15 kv, specimen current of 25 nA, and a beam size of 5–10 μm were used for quantitative analysis. Textural features were examined as back-scattered electron (BSE) images with the same microprobe but using a higher specimen current (>30 nA) and a rastered, focused beam. Vesicle walls of some samples were examined with a field emission Scanning Electron Microscope (SEM, LEO 982) at the U.S. Geological Survey in Menlo Park.

Sample sites

Volcaniclastic samples were collected at four sites (Fig. 1, Table 1). Site 1, the southernmost one, was sampled by 26D and then explored on dive S502. This site (Fig. 2A) consists of a cluster of steep-sided cones that form a partial ring (~3 km across) around a low shield about 0.5 km across and 25 m high (Clague et al. 2002). Dive observations show that two of the steep cones consist mainly of contorted vesicular pillow lava interbedded with thin layers of volcaniclastic deposits (see Fig. 12D of Clague et al. 2002). Dive samples S502-6A and-6B, and S502-8 were collected on the flanks of one cone at 4,202 and 4,038 m depth, respectively. Sample S502-11 was collected at 4,066 m on the adjacent cone located to the southeast (Fig. 2A). Dredge 26D (Clague et al. 1990) was also located in this general area, extending along a 4-km-long track on the sea floor just east of these cones over a depth range from 4,335 to 4,270 m.

Site 2, explored on dive S503, is a low shield volcano, about 80 m high (Fig. 2B), that is located 40 km north of dive site S502. The shield has a pit crater, located about 0.8 km to the east of the shield's summit, that is roughly 1.1 by 1.2 km across at the rim and 300 m deep. The bottom of the pit crater is covered with sediment and dense, angular basalt blocks up to 5 m across (Clague et al. 2002). A single volcaniclastic sample (S503-5H) was collected near the rim of the pit crater at 4,360 m depth.

Loosely cemented volcaniclastic samples were collected at a third site, located ~20 km to the northeast of dive site S502, during dive S704 (Fig. 2C). The volcaniclastic deposit was sampled at the base between two cones at 4,285 m depth. The northern cone, explored by the dive, is a low, nearly circular shield with a central crater. The southeastern cone is an elongate, steep sided ridge. Dredge 24D, located at the western base of the elongate ridge, recovered only pillow lava fragments of nephelinite composition (Clague et al. 1990).

The fourth site, located about 10 km east of the *Shinkai* 503 dive site, was not surveyed with the submersible. SeaBeam bathymetry (Fig. 2D) shows hummocky topography with hills 50 to 200 m high, that Clague et al. (1990) inferred to be vent structures. Volcaniclastic samples were recovered in dredge 27D on the sea floor east of the hills in water depths ranging from 4,187 to 3,900 m.

Sample descriptions

Site 1: Cluster of cones around low-relief shield

Three samples from dive S502 (-6A, -8, -11) are similar volcaniclastic breccia consisting of angular crystalline and glass fragments with interstitial pelagic clay (Table 1, Fig. 3A). These samples are clast-supported with minor pelagic clay and silt or yellow to orange clay and palagonite filling spaces between the clasts (Table 1). Some, if not all, of the palagonite and clay are probably replacing fine ash, although shapes of separate grains are rarely distinguishable. The samples are poorly sorted with fragments typically ranging in size from <1 mm to 1 cm, but rare crystalline basalt clasts up to 6 cm occur in sample S502-8. Some of the crystalline fragments have glass rinds. Glass rinds and glass grains are commonly rimmed by palagonite that ranges from a few microns to several millimeters thick (Fig. 4A). Both crystalline and glass fragments are highly vesicular and have many coalesced vesicles (Fig. 4B). Vesicularity measured with image-processing software of five of the most vesicular, larger (>1 cm) clasts ranged from 62 to 70%. Many of the smaller glass fragments (< 1 mm) are sparsely or non-vesicular, but typically have curved margins, indicating that they have broken across vesicles. Euhedral olivine microphenocrysts are present in most of the larger fragments. Minute, euhedral FeS crystals are evenly distributed on the inside of many vesicles, but are especially prominent in sample S502-11 (Fig. 5). The surfaces inside these vesicles have a slightly folded to undulating texture (Fig. 5).

Sample S502-6B, collected at the same location as S502-6A, consists of a volcaniclastic horizon, about 5 cm thick, adhering to a highly vesicular lava sample. This horizon is finer and shows more distinct layering, with graded bedding, compared to the other samples from this dive. One layer, presumably the bottom, consists of larger, angular, vesicular glass fragments (<1 cm) grading into a layer of thin, curved plate-like glass shards and thin (~0.05 mm) strands of glass in a matrix of manganese oxide (Fig. 4C), presumed to be of hydrothermal origin. Nearly all of these glass fragments have been altered to palagonite, but they have curved shapes and resemble limu o Pele. These slightly curved plates range from 0.3 to 1 cm long in cross section and are 0.03 to 0.1 mm thick. The Mn-oxide-cemented layer grades into a third layer of yellow-orange clay with disseminated Mn-oxide that contains only a small amount of elongate curved palagonite shards. In both layers, the curved shards are sub-parallel in alignment. The curvature measured for twenty random limu o Pele fragments indicates that the bubbles did not exceed 1 cm in diameter and had wall thicknesses ranging from 0.03 to 0.05 mm.

Volcaniclastic samples (26D) dredged from near the S502 dive site (Fig. 2A) are similar volcanic breccia consisting of angular, highly vesicular, crystalline and glass fragments with pelagic clay in the interstices. Although clast-supported, like those recovered on dive S502, they have a larger proportion of smaller glass grains (<1 mm) and a larger proportion of pelagic clay in the interstitial spaces than the typical S502 dive sample. Each of the three dredged samples (D26-6, -7, -8) shows a more-or-less well-developed stratification although none as pronounced as for S502-6B. These samples are also clast-supported layers of larger (mm to cm-size) fragments grading into progressively smaller grains in a more clay-rich matrix. This stratification is best developed for sample 26D-7 in which the lower clast-supported layer grades into a layer consisting mostly of silt and clay, almost devoid of glass grains (Fig. 4D). Unlike sample S502-6B with the yellow-orange, probably hydrothermal clay, the matrix of 26D-7

Table 1 Descriptive summary of North Arch volcaniclastic samples

Sample	Latitude (N) Longitude (W)	Water depth (m)	Glass composition	Fabric/ texture	Clast sizes (cm)	Clast shapes	Vesicle abundance	Vesicle shapes	Comments
502-6	23°35.53′ 157°42.98′	4,202	Basanite	Clast-supported Scoria	<0.5–2	Highly irregular, curved margins	High	Small (~0.5 mm) round, bigger ones (>1 mm) elongate	Concentric rims of palagonite, olivine microphenocrysts
502-6B	23°35.53′ 157°42.98′	4,202	Low-K alk.basalt	Layered and graded bedding	<0.01–0.3	Droplets, ribbons, Pele′s hair, limu	Low	Irregular	Aligned glass shards, hydrothermal Mn & Fe-rich clay matrix
502-8	23°35.47′ 157°42.58′	4,038	Basanite	Clast-supported scoria	<0.5–4	Angular to blocky	Mod. to high	Round to elongate	
502-11	23°35.39′ 157°42.46′	4,066	Basanite	Clast-supported scoria	<0.5–3	Angular with rounded corners	Mod	Round to elongate	Thin palagonite rims
503-5H	23°56.67′ 157°40.85′	4,348	Med-K alk. basalt, basanite	Matrix-supported glass sand, lithic fragments	<0.1–0.5	Angular to sub-rounded	None		Sharp contact with lava, lithic clasts
704-6	23°41.35′ 157°27.57′	4,285	Nephelinite	Poorly consolidated layer of glass shards	<0.1–0.5	Angular, ribbons, limu, Pele′s hair	Low to high	Round to elongate	Some tack welded to themselves
26D-6	23°35.1′ 157°42.3′	4,303	Low-K, med-K alk.basalt, basanite	Faint bedding and grading	<0.1–2	Angular, ribbons, droplets, Pele′s hair	High	Round to elongate	Fluidal clasts in fine size fraction
26D-7	23°35.1′ 157°42.3′	4,303	Low-K, med-K alk.basalt, basanite	Clast-supported scoria, very poorly sorted	<0.5–1	Highly angular, limu, droplets	High	Elongate and coalesced	Fluidal clasts inter stitial between lapilli
26D-8	23°35.1′ 157°42.3′	4,303	Low-K, med-K alk.basalt, basanite	Clast-supported scoria	<0.5–3	Angular, rounded corners	Mod. to high	Elongate	Reddish palagonite in matrix
27D-7A	23°54.3′ 157°34.9′	4,044	Med-K alk.basalt, basanite	Clast-supported scoria	<0.1–2	Angular, rounded corners	High	Round, elongate, coalesced	Reddish palagonite in matrix
27D-7B	23°54.3′ 157°34.9′	4,044	Med-K alk.basalt, basanite	Clast-supported scoria	<0.1–1	Angular, rounded corners	High	Round, some coalesced	Reddish palagonite in matrix

502, 503, and 704 are Shinkai 6500 samples. 26D and 27D are dredge samples collected on U.S. Geological Survey cruise F11-88-HW. Dredge locations averaged
Vesicle abundance estimated: high >50%, moderate 30–50%, low <30%

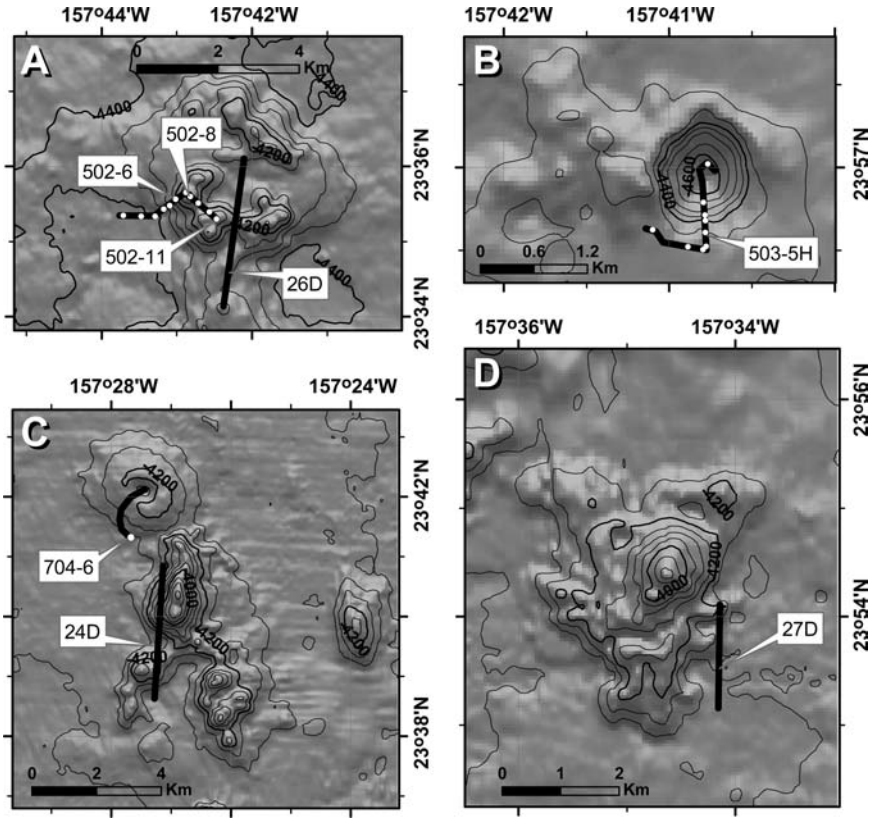

Fig. 2 Shaded relief images of SeaBeam bathymetry of the volcanic field: **A** site 1, showing location of *Shinkai* dive 502 and dredge 26, **B** site 2, showing location of dive 503, **C** site 3, showing location of dive 704 and dredge 24, and **D** site 4, showing location of dredge 27. Volcaniclastic sample numbers are indicated along the dive tracks. Contour interval is 20 m. Modified from Clague et al. (2002)

consists of pale brown pelagic marine clay. The finer grain size portions (< 1mm) of most of the 26D samples contain abundant fluidal-shaped glass shards, thin ribbon-like and fibrous strands resembling Pele's hair, and thin, elongate curved fragments which we interpret to be cross-sections of limu o Pele fragments (Fig. 6). Limu o Pele fragments in sample F11-26D-7 range from 0.3 to 1.3 cm in length and from 0.05 to 0.1 mm in thickness. In addition, there are numerous glass spheres (∼ 0.1 mm) that appear to be cross sections of glass droplets (Fig. 6C-F). The glass of many of these particles is partially or completely replaced by palagonite but grains with fresh glass cores exist.

Site 2: Shield with pit crater

The single volcaniclastic sample from dive S503 consists of a layer several cm thick of glass and crystalline fragments (<5 mm) adhering to a crystalline lava fragment (Fig. 4E). The fragments are dispersed in a matrix of pelagic sediment. The glass fragments are angular, blocky and dense, and some, but not all, have a rim of palagonite. Olivine microphenocrysts are present in some of the larger glass and crystalline fragments. The volcaniclastic layer is in sharp contact with the non-vesicular, holocrystalline, olivine-phyric lava fragment that does not have a glass rind (Fig. 4E). The small crystalline clasts in the volcaniclastic layer and the attached lava fragment have similar texture and mineralogy, suggesting they are fragments of the same lava flow.

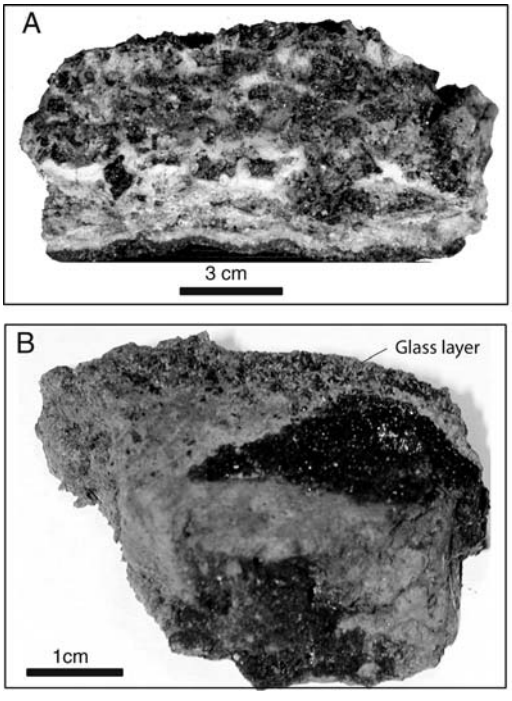

Fig. 3 **A** Typical volcaniclastic basanite sample recovered on *Shinkai* dive 502 at site 1. **B** Poorly consolidated sample from dive 704 recovered at site 3. This sample has a layer consisting mostly of limu o Pele glass shards along the upper margin. Note the highly vesicular lava fragment below the glass shard layer

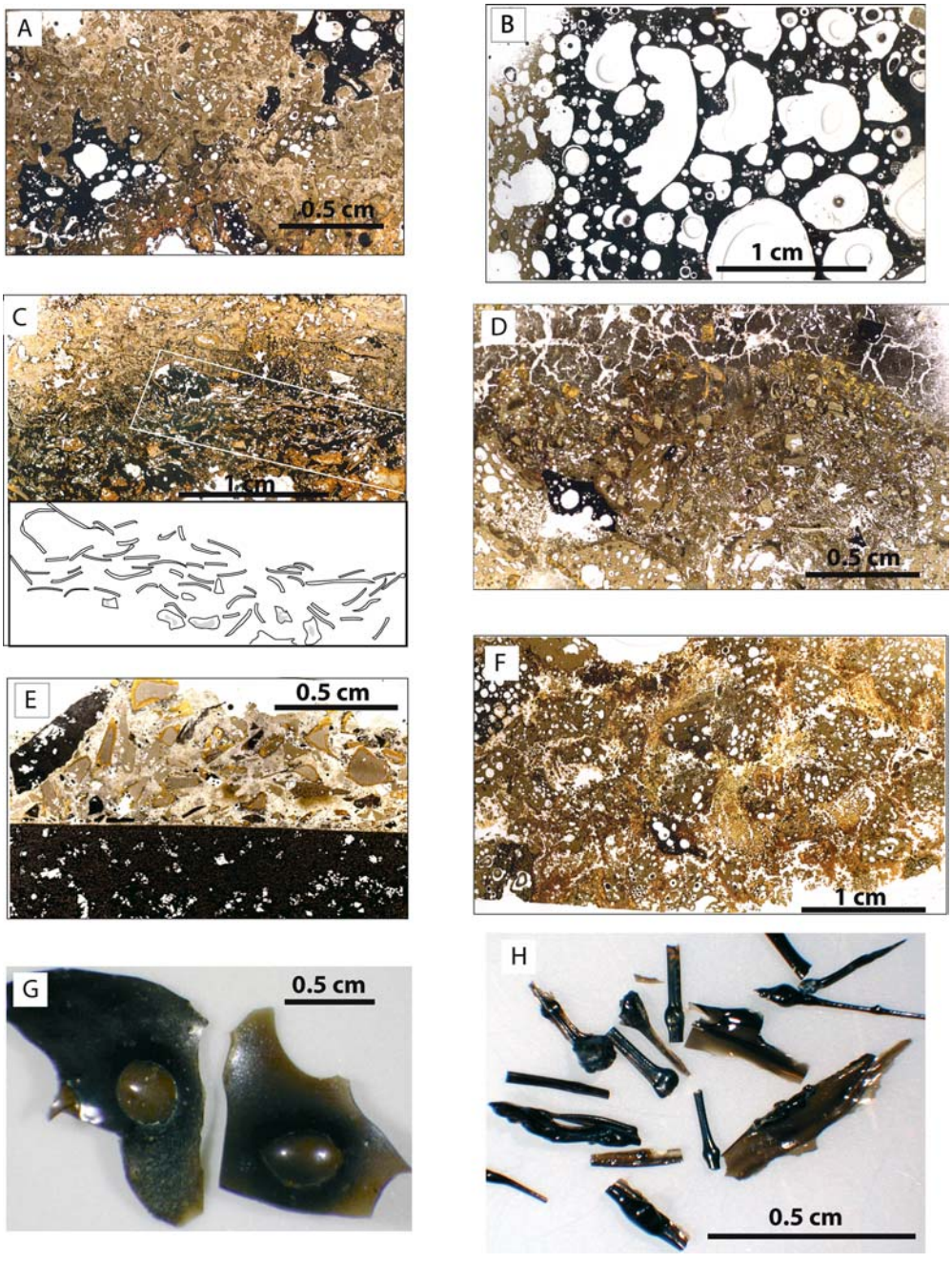

Fig. 4 Photomicrographs of volcaniclastite. **A** Typical basanite thin section (502-6A) from site 1, consisting of angular, vesicular pyroclasts of tachylitic (*black*) and fresh glass (*brown*) with interstitial pelagic clay (*tan*). **B** Pillow rim glass from dive 502, showing coalesced vesicles. **C** Alkalic basalt sample 502-6B with layers of curved, palagonitized glass shards, believed to be limu o Pele, in an altered matrix of yellow-brown clay (*upper margin*) and Mn-oxide (*black*) below. *Large white areas* are holes where material was plucked-out during thin section preparation. *Box* indicates area shown below with traced outlines of limu o Pele fragments. **D** Layered dredge sample 26D-7, site 1, showing progressively smaller grains upwards into a clay layer. **E** Dive sample 503-5H, site 2, consisting of non-vesicular, angular grains dispersed in a clay matrix in sharp contact with olivine-phyric lava. **F** Dredge sample 27D-7a, site 4, is composed mostly of vesicular, angular pyroclasts similar to those in the dredge 26 and 502 dive samples. **G** Limu o Pele fragments in the loosely consolidated sample recovered on dive 704, site 3, and **H** other fluidal shapes and Pele′s hair in sample S704-6

Site 3: Base between two cones

The poorly consolidated volcaniclastic sample recovered on S704 consists of a bedded, pelagic silt and sand layer with dispersed glass fragments and rare, large (~3 cm), highly vesicular, crystalline fragments (Fig. 3B). This layer grades into a dense glass-rich layer (~0.5 cm) consisting of angular glass fragments and abundant limu o Pele and Pele's hair-like or spindle-shaped fragments (Fig. 4G-H). The three-dimensional view easily allows distinguishing between limu o Pele and Pele′s hair-like shapes that may appear similar in the two-dimensional view observed in

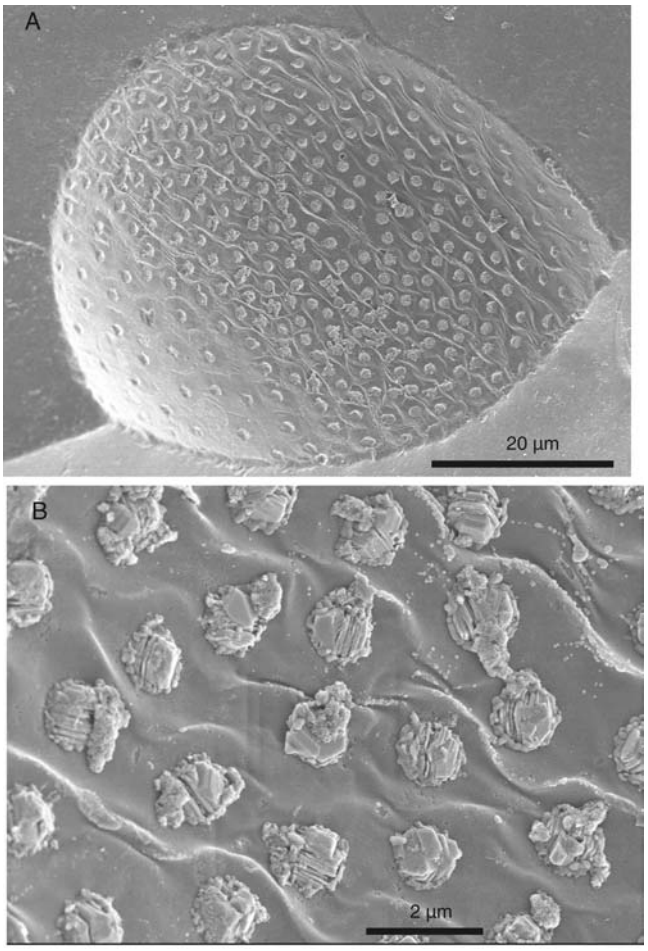

Fig. 5 Scanning electron microscope (SEM) image of: **A** a single vesicle in dive sample S502-11 covered with many minute sulfide crystals, and **B** close-up of iron sulfide crystals

thin sections. The limu o Pele fragments are concentrated in thin layers (<0.5 cm) in which they are aligned parallel to bedding. The fragments are 0.3 to 1.5 cm across and 0.01 to 0.05 mm thick. The only particle observed with greater wall thickness (0.2-mm) is contorted and appears to be tack welded to itself. However, fragments are not agglutinated as occurs in true spatter. The curvature of thirty random limu o Pele shards corresponds to a range of bubble sizes from ~1 to 1.5 cm. Unlike those observed in sample S502-6B from site 1, the curved glass fragments are unaltered and many enclose small crystals and round or elongate bubbles (Fig. 4G), which impart a bumpy surface to the particles.

Site 4: Low relief hills

Volcaniclastic samples recovered in dredge 27D are similar to 26D and S502 dive samples from site 1, except they are not layered. They are clast-supported volcanic breccia consisting of angular, highly vesicular, crystalline and glass fragments with minor pelagic clay in the interstices (Fig. 4F). Glass fragments are typically rimmed by palagonite. Rare curved glass fragments observed in cross section may be limu o Pele fragments. No glass spheres or Pele's hair-like strands were observed.

Vesicularity determined for the five most vesicular, larger (>1 cm) clasts in samples from this site is comparable to that observed for pyroclasts at site 1. A maximum vesicularity of 70% was determined at both sites, and exceeds the maximum vesicularity of 56% observed for samples of pillow basalts from the same sites (Dixon et al. 1997).

Glass compositions

Representative analyses of 180 glass grains are given in Table 2 and analyses are shown in Fig. 7. Analyses may be of a single spot if the sample is small or if only unaltered cores remain or up to six analyses may have been averaged for the larger, highly vesicular scoria fragments.

Site 1: Cluster of cones around low-relief shield

Glass compositions of volcaniclastic samples collected on dive S502 are alkalic basalt and basanite. The samples from the flanks of the western cone (S502-6A, -8), as well as sample S502-11 from the adjacent cone, are basanite with a narrow compositional range (MgO from about 7.8 to 7.0 wt%, Fig. 7A). Sample S502-6B, collected at the same site as the basanite S502-6A, consists entirely of low-K_2O (~0.4-0.6 wt%) alkalic basalt. Glass grains within the presumed lower layer of this sample are typically relatively primitive with MgO >9 wt% but with a range from about 10.4 to 7.5 wt% MgO (Fig. 7A). The many limu o Pele and ribbon-shaped fragments in the finer-grained layer are typically replaced by palagonite but the remaining fresh cores in some of these are also low-K_2O alkalic basalt, identical to the angular glass fragments. Sulfur is typically high in all, consistent with deep-sea eruption, but it has a considerable range (~900 to 1,600 ppm) at similar K_2O contents (Fig. 7B). Cl is typically higher in the basanite (~700 to 1,200 ppm) but overlaps with that of the alkalic basalt (~400 to 900 ppm) and also has a considerable range over narrow K_2O contents (Fig. 7C).

The 26D volcaniclastic samples include basanite and low-K_2O alkalic basalt similar to those collected on dive S502, but also include some higher K_2O (>0.6 wt%) alkalic basalt. The basanite clasts are generally more fractionated (MgO=6.5-7.0 wt%) than those from dive S502. The unaltered glass spheres and the Pele's hair-like fragments are all low-K_2O alkalic basalt with MgO contents ranging from 7 to 10.3 wt%. S and Cl (Fig. 7B, C) span a slightly larger range than for the dive samples, with maxima of 1800 and 1300 ppm, respectively. In contrast, limu o Pele fragments are present as low- and high-K_2O alkalic basalt as well as basanite. Their S and Cl contents are similar to those of the angular glass grains with comparable K_2O contents.

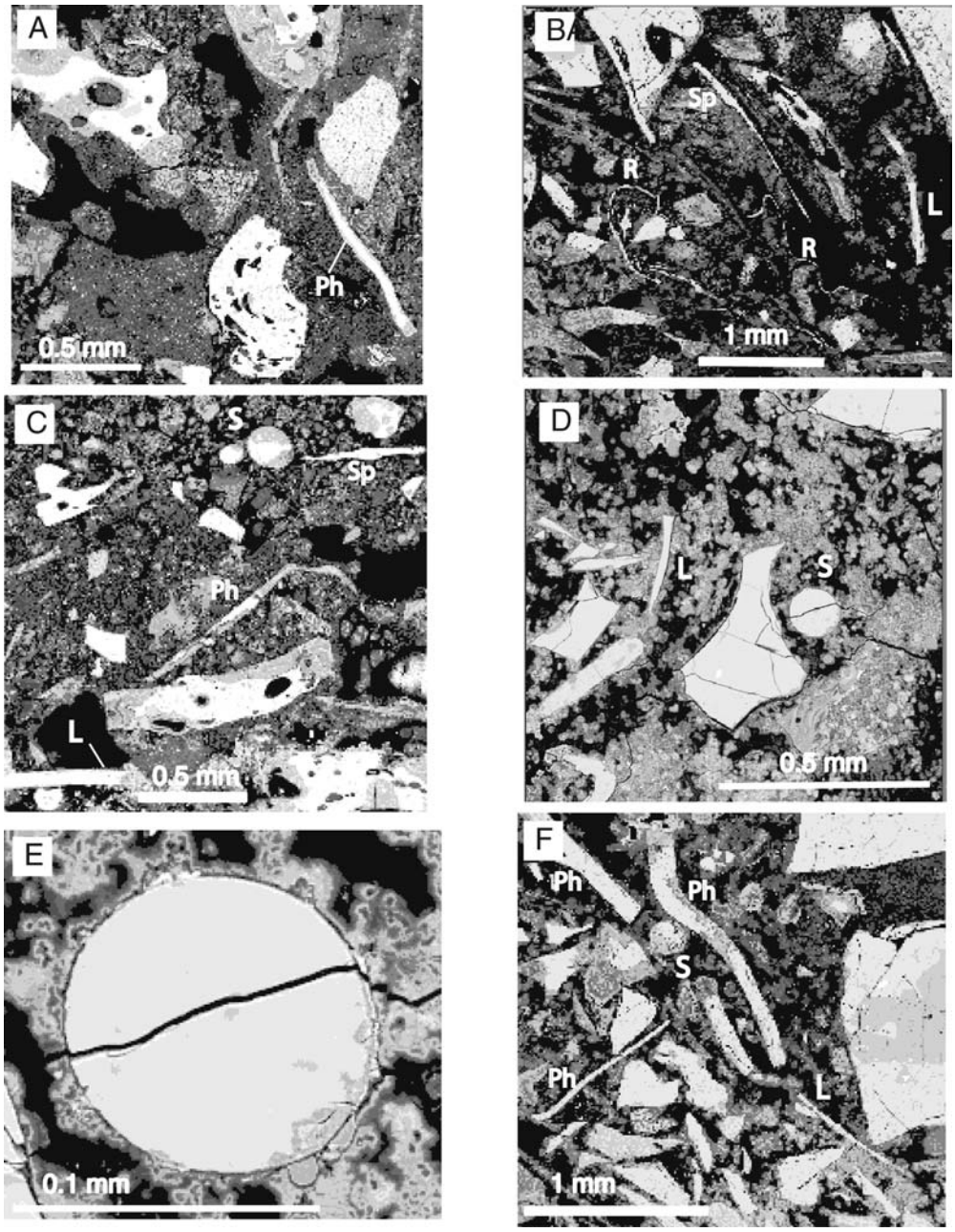

Fig. 6 Back scattered electron (BSE) images of fluidal and curved glass fragments (*white*) in finer-grain sized portion of dredged volcaniclastite (26D) from site 1. Some Pele′s hair-like fragments (*Ph*), curved glass shards that are presumably limu o Pele (*L*), spindle (*Sp*) and ribbon shapes (*R*) as well as circular cross sections of droplet shapes (*S*) have been identified. **A** Vesicular pyroclasts with deformed vesicles and curved margins suggesting breakage across vesicles. **B** Thin, contorted, ribbon shapes, limu o Pele, and angular glass grains, **C** partially altered (*gray*) glass sphere, limu o Pele, and spindle shaped fragments, **D** unaltered glass sphere and **E** close-up of sphere shown in (D). **F** Partially altered sphere, limu o Pele and Pele′s hair amidst angular, dense glass fragments, some of which contain euhedral olivine crystals (*pale gray*)

Site 2: Shield with pit crater

Glass fragments in the volcaniclastic layer of sample S503-5H have three distinct compositions. Two basanite compositions occur, one of which is less evolved (MgO ~9 wt%) than the other (MgO ~7.5 wt%). The third composition is high-K_2O alkalic basalt with MgO ranging from 7.4 to 8.0 wt% (Fig. 7A). Sulfur is typically high (1,300 to 1,800 ppm) in all but shows a considerable range for each compositional group (Fig. 7B). Cl is slightly higher in the basanite compositions but also shows a large range at a given K_2O (Fig. 7C).

Site 3: Base between two cones

The glass in the volcaniclastic sample from S704 is nephelinite, ranging in MgO from 9 to 7.5 wt% (Fig. 7A). S and

Table 2 Representative electron microprobe analyses of glass

Sample	502-6A	502-6A	502-6B	502-6B	502-6B	502-6B	502-8	502-11	503-5H	503-5H	503-5H	704-6	704-6	704-6
Type	L	Pc	L	Pc	Pc	Pc	Pc	Pc	G	G	G	L	L	L
(wt%)	B	B	AB	AB	AB	AB	B	B	B	AB	B	N	N	N
SiO_2	44.4	44.2	46.2	46.2	46.3	46.3	44.2	44.1	45.1	46.5	45.3	42.0	42.1	41.4
AL_2O_3	14.7	14.3	13.8	14.3	14.4	14.8	14.4	14.4	13.9	15.1	14.3	13.2	13.3	13.4
FeO	12.0	12.0	11.9	11.9	11.6	11.8	11.9	11.9	12.0	11.4	12.2	12.8	12.8	13.2
MgO	7.20	7.59	10.3	9.09	9.33	7.70	7.00	7.56	9.29	8.04	7.52	9.03	8.14	7.62
CaO	12.9	12.8	11.0	11.4	10.9	12.0	13.1	12.8	11.8	11.9	11.5	13.1	13.3	13.3
Na_2O	3.74	3.71	2.96	3.11	3.07	3.09	3.71	3.70	3.16	3.32	3.68	3.83	3.95	4.22
K_2O	1.09	1.11	0.45	0.48	0.50	0.52	1.12	1.10	1.03	0.66	1.02	1.23	1.26	1.33
TiO_2	2.38	2.45	1.51	1.62	1.61	1.69	2.37	2.34	2.27	2.00	2.79	2.44	2.47	2.74
P_2O_5	0.57	0.56	0.26	0.27	0.27	0.27	0.53	0.56	0.43	0.34	0.40	0.64	0.66	0.65
MnO	0.21	0.16	0.14	0.16	0.16	0.19	0.18	0.20	0.23	0.19	0.16	0.19	0.20	0.17
Cl	0.11	0.10	0.05	0.07	0.08	0.09	0.11	0.10	0.06	0.06	0.04	0.09	0.10	0.10
S	0.14	0.12	0.15	0.12	0.16	0.12	0.12	0.12	0.16	0.16	0.15	0.10	0.9	0.13
Total	99.4	99.1	98.7	98.7	98.4	98.6	98.7	98.9	99.4	99.7	99.1	98.7	99.2	98.3
Sample	26D-6	26D-6	26D-6	26D-6	26D-7	26D-7	26D-7	26D-7	26D-8	26D-8	26D-8	27D-7a	27D-7a	27D-7a
Type	L	S	Pc	Pc	S	L	Pc	Ph	S	L	Pc	Pc	L	Pc
(wt%)	AB	AB	AB	B	AB	AB	B	AB	AB	AB	B	B	AB	B
SiO_2	46.5	46.9	45.0	44.0	46.9	47.0	44.8	47.3	45.6	46.9	44.6	44.0	45.8	44.2
AL_2O_3	14.2	14.0	13.6	14.6	14.1	14.0	14.6	15.1	13.9	15.1	14.7	14.4	13.8	14.5
FeO	11.7	11.8	12.8	12.1	11.9	11.4	12.4	11.7	12.9	12.3	12.5	11.7	12.5	12.0
MgO	9.79	9.36	10.1	6.87	9.22	10.0	6.65	6.73	9.68	7.81	6.78	6.78	9.02	7.00
CaO	11.2	11.2	10.9	13.1	11.6	10.8	13.4	12.6	11.4	12.1	13.4	13.0	11.6	13.2
Na_2O	3.05	2.99	3.27	3.71	2.97	2.84	3.64	3.16	3.20	2.99	3.87	3.73	3.11	3.83
K_2O	0.49	0.52	0.71	1.14	0.52	0.44	1.11	0.61	0.64	0.55	1.13	1.12	0.61	1.17
TiO_2	1.61	1.68	2.13	2.38	1.75	1.41	2.47	1.99	2.09	1.88	2.53	2.39	1.89	2.36
P_2O_5	0.28	0.30	0.34	0.54	0.29	0.27	0.51	0.30	0.28	0.25	0.47	0.45	0.38	0.54
MnO	0.20	0.17	0.14	0.16	0.20	0.14	0.17	0.19	0.18	0.24	0.19	0.17	0.18	0.16
Cl	0.06	0.08	0.05	0.13	0.06	0.05	0.11	0.06	0.11	0.07	0.12	0.10	0.09	0.11
S	0.10	0.18	0.12	0.14	0.16	0.12	0.16	0.16	0.13	0.18	0.17	0.12	0.18	0.14
Total	99.2	99.2	99.2	98.9	99.7	98.5	100.0	99.9	100.1	100.4	100.5	98.0	99.2	99.2

L limu; *S* sphere; *Pc* vesicular pyroclasts; *Ph* Pele's hair; G reworked, in sediment. *B* basanite; *AB* alkalic basalt; *N* nephelinite

Cl contents are similar to the basanite from site 1, ranging from 900 to 1,300 ppm, and 850 to 1,150 ppm, respectively. The compositions are similar to, but higher in K_2O, than the nephelinite lava samples recovered in nearby dredge 24D at the base of the elongated ridge (Clague et al. 1990).

Site 4: Low relief hills

Except for two grains of high-K_2O alkalic basalt glass, the glass in the volcaniclastic deposit sampled by dredge 27D is evolved basanite with MgO <7.0 wt%. Cl and S (Fig. 7B, C) are within the range observed for the basanite from site 1. The two alkalic basalt grains have variable S (1,200 to 1,800 ppm) but similar Cl (800 to 900 ppm) at comparable K_2O contents.

Comparison with associated lava samples

The compositions of volcaniclastic grains greatly expand information on compositional diversity compared to those obtained only from lava samples at each site. Similar to the volcaniclastic grains, the glass rinds on pillow lava collected at site 1 are also mostly basanite and lesser alkalic basalt of both low- and high-K_2O. The basanite pillow rinds have a compositional range comparable to the glass grains but the alkalic basalt lava rinds include some considerably more evolved compositions, with MgO as low as 5.8 wt% (Clague et al. 1990, off scale in Fig. 7A). Compositions of pillow lava at site 2 include more evolved basanite and less evolved high-K_2O alkalic basalt, which are not represented in the fine glass fragments of sample 503-5H (Fig. 7).

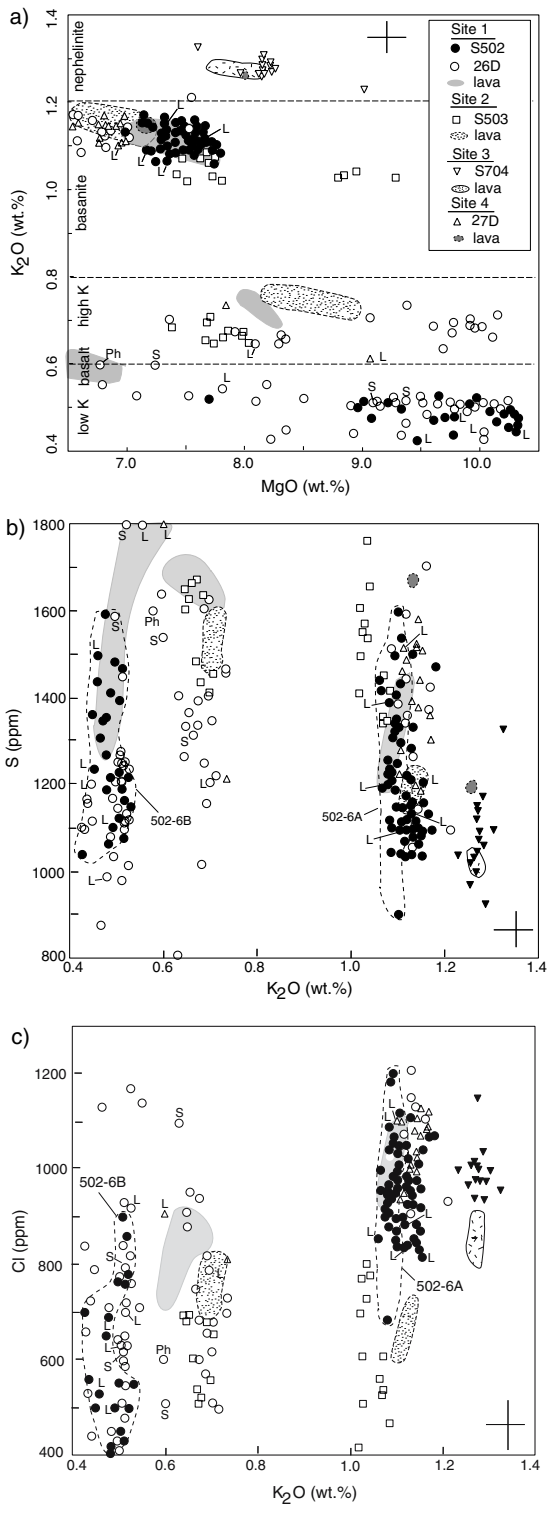

Fig. 7 Composition of glass fragments. **A** K_2O vs. MgO shows the range of compositions recovered at each site. **B** S vs. K_2O and (C) Cl vs. K_2O. S and Cl show a large range in abundance at similar K_2O contents. Compositions of dense limu oPele (*L*), glass spheres (*S*) and Pele′s hair (*Ph*) are indicated. All other analyses are of highly vesicular pyroclasts. Compositions of associated pillow lava rinds are shown as fields. Note that fields shown in **C** are for dive samples only. Data for lava are from Clague et al. (1990, 2002), and for S704 from M. Coombs (personal communication). *Error bars* are one standard deviation

Compositions of pillow rinds from S704 are nephelinite with a limited range in MgO (7.4–8.2 wt%), suggesting they are from a single flow. Compared to the pillow rinds, the volcaniclastic compositions span a larger range in MgO and include more volatile-rich (higher S and Cl) compositions. Lava samples recovered in dredge 27D include two basanite (∼7 wt% MgO) and one nephelinite sample. The basanite samples are similar to the volcaniclastic samples, but at the low-MgO end of the spectrum. The nephelinite composition is not represented in the volcaniclastic samples but it is compositionally similar to samples from dive S704.

S and Cl contents of all analyzed glasses, whether they are volcaniclastic or pillow rinds, show no correlation with vesicle abundance. Both elements have a narrower compositional range in the pillow rinds compared to the large range observed for volcaniclastic grains at comparable K_2O.

Discussion

Fragmentation

Due to the great eruption depths that make water vaporization impossible (Bischoff and Rosenbauer 1988), steam generated from trapped seawater cannot be the mechanism causing magma fragmentation. Supercritical water at these depths has low density (approximately 68 kg/m^3, calculated using the Peng-Robinson cubic equation of state; Peng and Robinson 1979) compared to the surrounding unheated seawater, but the expansion is not instantaneous since no phase change is involved (Clague et al. 2003b). The theoretical model of Wohletz (2003) for explosive hydrovolcanism at pressures greater than the critical point for seawater vaporization proposes that a supercritical fluid film forms at the water/magma contact surface. Repeated film collapse imparts kinetic energy and causes magma fragmentation. Typical submarine eruptions involve large water to magma ratios, resulting in rapid heat dissipation, so special conditions that produce low water/magma ratios appear to be required for Wohletz′s (2003) model. Entrapment of water within narrow vent conduits, beneath lava flows, or by engulfment during rapid extrusion may result in favorable water/magma ratios and some of these conditions undoubtedly existed for the North Arch eruptions. The Wohletz (2003) model did not address shapes and sizes of fragments generated. However, fragmentation resulting from kinetic energy associated with film collapse would most likely produce dense, angular shards rather than the fluidal and bubble-wall shapes observed. Explosive fragmentation due to discharge of a magmatic volatile-rich supercritical fluid appears to be the most viable mechanism for the origin of volcaniclastic deposits in the North Arch volcanic field.

Fluidal pyroclasts, including glass droplets, thin strands resembling Pele's hair, ribbon-like strands, and limu o Pele fragments occur in deposits at sites 1, 3, and 4, although they are rare and generally smaller relative to the angular, vesicular pyroclasts in these deposits. They have alkalic basalt, basanite, and nephelinite compositions but they

appear to be more abundant in less evolved compositions (MgO >9 wt%). Such fluidal clast morphologies, with the exception of the limu o Pele fragments, are similar to those generated in subaerial lava fountains driven by magmatic gas discharge or in phreatomagmatic eruptions (e.g.Vergniolle and Mangan 2000).

Littoral Kilauean lava bubbles are formed by steam derived from trapped seawater and they can reach diameters of 5 to 10 m within seconds (Mattox and Mangan 1997). Similar in shape but smaller in size, limu o Pele shards collected from Loihi Seamount and Kilauea′s east rift zone from about 1,200 m depth (Clague et al. 2000) have an average diameter of about 5.9 cm. At Seamount 6, near the East Pacific Rise, curvature of similar limu o Pele shards collected from 1,700 to 2,000 m depth indicate an average bubble diameter of only about 2.2 cm (Maicher and White 2001). Bubble size of North Arch samples, from over 4,000 m depth, is still smaller with a maximum diameter of only 1.5 cm. Based on this limited sampling, the size of bubbles appears to decrease progressively with increasing water depths. However, wall thicknesses of North Arch limu o Pele fragments, ranging from 0.03 to 0.1 mm with an average of 0.05 mm, appear similar to those from Loihi (<0.05 mm, Clague et al. 2000). Wall thicknesses of North Arch limu o Pele overlap with those from Seamount 6, which range from 0.05 to 0.43 mm, with an average of 0.14 mm (Maicher and White 2001).

The presence of limu o Pele fragments in alkalic basalt, basanite, and nephelinite suggests that bubbles were able to stretch lava surfaces regardless of composition and over a range of low viscosities (∼1.2 to ∼7 Pa s, Dixon et al. 1997). The compositions of limu o Pele fragments are similar to those of angular glass grains and rinds of pillows from the same site, suggesting that discharge in bursts of a supercritical, volatile-rich, low density fluid phase occurred, and probably initiated, most of the eruptions. Hence, we propose that primary fragmentation in North Arch volcaniclastite most likely resulted from Strombolian-like activity related to release of bursts of a volatile-rich, low-density, magmatic fluid phase. Additional fragmentation due to cooling-contraction granulation probably occurred as well.

Magmatic degassing

High vesicularity of pyroclasts and lava from the steep cones unequivocally indicates extensive exsolution of magmatic volatiles, primarily CO_2 (Dixon et al. 1997), despite great water depth. Limu o Pele and Pele′s hair-like fragments, spindle and ribbon shapes, and glass droplets are inferred to indicate at least mildly explosive eruptions at water depths >4,200 m. In a shallow water or subaerial environment, the highly volatile-charged magma would have erupted in gas-driven columns of great height. In more than 4,000 m of seawater, the high hydrostatic pressure (>40 MPa) would have limited the height of fountains and eruption columns by suppressing gas formation. Quenching in cold water would have prevented welding and agglutination of spatter, commonly observed in subaerial deposits.

Dixon et al. (1997) used the sum of volatiles dissolved in glass plus those required to produce the observed volume of vesicles to estimate a bulk volatile content for North Arch basanite of 5.4 wt% CO_2 and 1.9 wt% H_2O. Head and Wilson (2003) recently modeled submarine pyroclastic eruptions and used these values to calculate a maximum depth of 2,134 m at which explosive eruption would be possible for a North Arch basanite. However, the pyroclastic deposits described herein were generated by explosive eruptions that occurred at about twice that depth.

There are at least two ways to resolve this dilemma. The first would require that about half the magmatic volatiles have completely escaped from the magma without leaving vesicles and thus are unaccounted for in the Dixon et al. (1997) calculations. The second requires accumulation of bubbles from a larger volume of magma than that erupted. The first solution requires that the initial volatile contents are therefore roughly twice the already high contents estimated by Dixon et al. (1997). Many of the smaller pyroclasts have curved margins suggesting they are broken fragments of larger vesicular clasts. Their vesicularity, and therefore their initial volatile contents, may have been underestimated. However, vesicularity of single pyroclasts within a given sample can be quite variable, ranging from nearly vesicle free for the smallest grains to a maximum of 70%. These values are in good agreement with the vesicularities of lava samples measured by Dixon et al. (1997) and with their closed system degassing curves. Hence, it is unlikely that Dixon et al. (1997) underestimated the initial volatile content by a factor of 2. We think it is more likely that the "missing" volatiles required for fragmentation of these alkalic magmas at such great ocean depths accumulated from a larger volume of magma, simultaneously forming a complementary, relatively volatile-poor magma, that erupted as long thin lava flows (Clague et al. 1990, 2002).

The second solution, involving accumulation of bubbles, has been explored by Head and Wilson (2003). They proposed two modes of bubble accumulation. In both cases, the low solubility of CO_2 in basaltic magmas leads to bubble nucleation and initial growth as magma migrates towards the Earth′s surface. The first mode results in the accumulation of magmatic volatiles at the top of a magma reservoir, and subsequent foam-layer collapse that drives Hawaiian-style fountains. This model has been questioned by Parfitt (2004). Regardless, it does not appear applicable to the North Arch volcanic field because the relatively primitive compositions of the basaltic lavas and the presence of mantle olivine xenocrysts are inconsistent with magma residence in long-lived shallow magma reservoirs in which magmas would be expected to fractionate to more evolved compositions, and xenoliths and xenocrysts would gravitationally settle (Clague 1987).

In Head and Wilson′s (2003) second mode of bubble accumulation, the volatile content is insufficient to cause fragmentation under Hawaiian-like conditions, but low magma rise speeds allow coalescence and more rapid rise of bubbles that drive Strombolian-like eruptions. This mode is usually associated with low eruption rates. Early-nucleated

bubbles overtake smaller, later-nucleated bubbles, in what Head and Wilson (2003) refer to as a runaway bubble coalescence process. The eruption style is characterized by intermittent discharge of large bubbles that disrupt magma and expel it directly from the vent. The bubble bursts should expel lava clots the size and morphology of which depend on bubble size, arrival speed at the surface, melt viscosity, and the degree of cooling. The scenario outlined by Head and Wilson (2003) differs somewhat from what we infer in that the limu o Pele shards are also formed during bubble bursts, perhaps by smaller explosions than those that form the larger pyroclasts. The second difference is that the runaway coalescence process described by Head and Wilson (2003) is inferred to produce dense blocky fragments. Many of the particles in the North Arch samples are highly vesicular, indicating that although some bubbles have coalesced into larger bubbles that disrupt the magma, these bubbles are still rising through magma rich in small bubbles. This difference is important since the fragments we observe are generally of ash and lapilli sizes, whereas the process they describe would mainly produce larger pyroclasts.

Some H_2O was included in the exsolved volatile phase, based on CO_2/H_2O mass ratios of 1 to 4 (Dixon et al. 1997). In addition to H_2O, some S and Cl exsolved from these melts and contributed to bubble formation. S contents, although considerably higher (to 1,800 ppm) than in MORB at comparable MgO, show losses of at least 400 ppm at a nearly constant K_2O for some compositions (Fig. 7B). Abundant minute sulfide crystals lining some of the vesicles (Fig. 5) in dive sample S502-11 confirm that S exsolved from the magma, and then reacted with Fe in the wall of the vesicle to form the sulfide crystals as the volatile phase cooled. The vesicle surfaces have an undulating texture (Fig. 5) that formed as the volatiles in the bubble cooled and contracted while the vesicle wall was still plastic. Even Cl, which shows only a weak positive correlation with K_2O (Fig. 7C), varies by more than 200 ppm over a narrow range of K_2O. Dixon et al. (1997) have shown an overall positive correlation of Cl with P_2O_5, reflecting the degree of partial melting. Considerably larger scatter than that expected due to analytical uncertainty suggests some loss of Cl from the melt may be possible during bubble formation when a supercritical fluid rather than a vapor phase exsolves. Alternatively, or in addition, seawater contamination may be a factor for pyroclasts with unusually high Cl contents. However, there is no visible alteration of the glass. Apparently exsolution of a CO_2-rich supercritical fluid phase can strip some of the higher solubility volatiles like S, H_2O, and perhaps Cl as well.

Eruption style and sequence

The massive- to crudely-bedded, clast-supported samples from sites 1, 3, and 4, consist of poorly sorted, angular, highly vesicular glass fragments, and are most likely primary pyroclastic deposits formed from proximal fallout (within tens of meters). The great hydrostatic pressure would have limited the height of eruption columns and formed the steep-sided cones that are rarely more than 50 to 200 m tall (Clague et al. 2002). Preservation of delicate limu o Pele and fluidal glass particles suggests little abrasion during transport. The fine grain size, grading, well-developed stratification and alignment of limu o Pele particles in sample S502-6B are consistent with deposition by settling from suspension at greater distances from the vent than for the coarser fall deposits. In contrast, the matrix-supported sample (503-5H), collected at the rim of the pit crater at site 2, consists of rare lithic fragments and angular, dense glass fragments of a variety of compositions that are most likely spalled glass rinds of lava. Dive observations of volcaniclastic deposits interbedded with pillow lava suggest explosive eruptions forming the small pyroclastic cones of the North Arch Volcanic Field were followed by, or were contemporaneous with, effusive eruptions of less volatile-rich pillow lavas. Pillow lava eruptions in turn were probably followed by effusive eruption of nearly vesicle-free, degassed sheet flows that traveled long distances over nearly flat terrain (Clague et al. 1990, 2002). The pervasive alteration of the curved glass fragments, and the matrix of yellow to orange clay with disseminated Mn-oxide of sample 502-6B, suggest prolonged contact with hydrothermal solutions. The thick palagonite rims on most pyroclasts may have formed post-depositionally as hydrothermal fluids circulated within the deposits.

Conclusions

The North Arch volcanic field includes pyroclastic deposits that erupted explosively despite water depths greater than 4,000 m. Massive to crudely bedded scoria deposits, comprising the bulk of the samples, were most likely deposited in close proximity to the source vents from eruption columns of limited height. Less common samples with graded bedding and finer grain size may have been deposited at greater distances from the vent. Glass droplets and Pele's hair-like strands testify to the presence of Hawaiian-style fire fountains. Ubiquitous limu o Pele fragments match the composition of angular fragments and associated pillow rinds, and probably formed during discharge of lava containing coalesced bubbles of exsolved magmatic volatiles. Lava compositions ranged from low-K_2O alkalic basalt to nephelinite. The presence of bubbles and coalesced vesicles in many samples suggests accumulation of a volatile phase, presumably CO_2. Release of slugs of the accumulated low-density, magmatic supercritical fluid rich in volatiles provided the driving force for Strombolian-like explosive eruptions.

Acknowledgments DAC thanks JAMSTEC, particularly Eiichi Takahashi, Jiro Naka, Kozo Uto, and the Shinkai 6500 Team for support in mapping and sampling the North Arch volcanic field in 2000 and 2002. We also thank Naoto Hirano for his observations and sample selection during Shinkai dive S704 and Michelle Coombs for providing some glass analyses of the S704 flow samples. Summer intern Stella Maceri helped cut and describe some of these samples as part of a hyaloclastite study. Robert Oscarson assisted with microprobe and SEM analyses, and Jenny Paduan and Nadine Golden in producing Fig. 1 and 2. Constructive reviews by James White,

Kathy Cashman, and Associate Editor Jocelyn McPhie improved the manuscript.

References

Bischoff JL, Rosenbauer RJ (1988) An empirical equation of state for hydrothermal seawater. Am J Sci 285:725–763

Cas RAF, Wright JV (1987) Volcanic successions, modern and ancient. Allen and Unwin, London, pp 1–528

Clague DA (1987) Hawaiian xenolith populations, magma supply rates, and development of magma chambers. Bull Volcanol 49:577–587

Clague DA, Dalrymple GB (1988) Age and petrology of alkalic postshield and rejuvenated stage lava from Kauai, Hawaii. Contrib Mineral Petrol 99:202–218

Clague DA, Davis AS, Bischoff JL, Dixon JE, Guyer R (2000) Lava bubble-wall fragments formed by submarine hydrovolcanic explosions on Loihi Seamount and Kilauea Volcano. Bull Volcanol 61:437–449

Clague DA, Frey FA (1982) Petrology and trace-element geochemistry of the Honolulu Volcanics, Oahu: implications for the oceanic mantle beneath Hawaii. J Petrol 23:447–504

Clague DA, Holcomb RT, Sinton JM, Detrick RS, Torresan ME (1990) Pliocene and Pleistocene alkalic flood basalts on the seafloor north of the Hawaiian Islands. Earth Planet Sci Lett 98:175–191

Clague DA, Uto K, Satake K, Davis AS (2002) Eruption style and flow emplacement in the submarine North Arch volcanic field, Hawaii. In: Takahashi E, Lipman PW, Garcia MO, Naka J, Aramaki S (eds) Hawaiian volcanoes: deep underwater perspectives. Am Geophys Union Monogr 128:65–84

Clague DA, Batiza R, Head JW III, Davis AS (2003a) Pyroclastic and hydroclastic deposits on Loihi Seamount, Hawaii. In: White JD, Smellie J, Clague DA (eds) Explosive subaqueous volcanism. Am Geophys Union Monogr 140:73–95

Clague DA, Davis AS, Dixon JE (2003b) Submarine Strombolian eruptions on the Gorda Mid-Ocean Ridge. In: White JD, Smellie J, Clague DA (eds) Explosive subaqueous volcanism. Am Geophys Union Monogr 140:111–128

Davis AS, Clague DA (2003) Hyaloclastite from Miocene seamounts offshore central California: compositions, eruption styles, and depositional processes, In: White JD, Smellie J, Clague DA (eds) Explosive subaqueous volcanism. Am Geophys Union Monogr 140:129–142

Davis AS, Clague DA, Friesen WB (1994) Petrology and mineral chemistry of basalt from the Escanaba Trough, southern Gorda Ridge. US Geol Surv Bull 2022:153–170

Davis AS, Clague DA, Bohrson WA, Dalrymple GB, Greene HG (2002) Seamounts at the continental margin of California: a different kind of oceanic volcanism. Geol Soc Am Bull 114:316–333

Dixon JE, Clague DA, Wallace P, Poreda R (1997) Volatiles in alkalic basalts from the North Arch volcanic field, Hawaii: extensive degassing of deep submarine-erupted alkalic series lavas. J Petrol 38:911–939

Eissen J-P, Fouquet Y, Hardy D, Ondreas H (2003) Recent MORB volcaniclastic explosive deposits formed between 500 and 1,750 m.b.s.l at the axis of the Mid-Atlantic Ridge. In: White JD, Smellie J, Clague DA (eds) Explosive subaqueous volcanism. Am Geophys Union Monogr 140:143–1408

Fisher RV (1961) Proposed classification of volcaniclastic sediments and rocks. Geol Soc Am Bull 72:1395–333

Fisher RV, Schmincke H-U (1984) Pyroclastic rocks. Springer, Berlin, Heidelberg New York, pp 1–472

Fouquet Y, Eissen JP, Ondréas H, Barriga F, Batiza R, Danyushevsky L (1998) Extensive volcaniclastic deposits at the Mid-Atlantic Ridge axis: results of deep-water basaltic explosive activity? Terra Nova 10:280–286

Frey FA, Clague DA, Mahoney JJ, Sinton JM (2000) Volcanism at the edge of the Hawaiian Plume: petrogenesis of submarine alkalic lavas from the North Arch volcanic field. J Petrol 41:667–691

Gill J, Torssander P, LaPierre H, Taylor R, Kaiho K, Koyama M, Kusakabe M, Aitchison J, Cisowski S, Dadey K, Fujioka K, Klaus A, Lovell M, Marsaglia K, Pezard P, Taylor B, Tazaki K (1990) Explosive deep water basalt in the Sumisu backarc rift. Science 248:1214–1217

Head JW, Wilson L (2003) Deep submarine pyroclastic eruptions: theory and predicted landforms and deposits. J Volcanol Geotherm Res 121:155–193

Hékinian R, Pineau F, Shilobreeva S, Bideau D, Gracia E, Javoy M (2000) Deep sea explosive activity on the Mid-Atlantic Ridge near 34°50′ N: Magma composition, vesicularity and volatile content. J Volcanol Geotherm Res 98:49–77

Hon K, Heiker C, Kjargaard JI (1988) Limu o Pele: a new kind of hydroclastic tephra from Kilauea Volcano, Hawaii. Geol Soc Am Abst Prog 20 (7):112–113

Maaloe S, James D, Smedley P, Petersen S, Garmann LB (1992) The Koloa volcanic suite of Kauai, Hawaii. J Petrol 33:761–784

Maicher D, White JL (2001) The formation of deep-sea Limu o Pele. Bull Volcanol 63:482–496

Mattox TN, Mangan M (1997) Littoral hydrovolcanic explosions: a case study of lava-seawater interaction at Kilauea volcano. J Volcanol Geotherm Res 75:1–17

Moore JG, Schilling JG (1973) Vesicles, water, and sulfur in Reykjanes ridge basalts. Contrib Mineral Petrol 4:105–118

Parfitt EA (2004) A discussion of the mechanisms of explosive basaltic eruptions. J Volcanol Geotherm Res 134:77–107

Peng D-Y, Robinson DB (1979) The calculation of three-phase solid-liquid-vapor equilibrium using an equation of state. Advances in chemistry series 182, Am Chem Soc, Washington, DC, pp 185–196

Reiners PW, Nelson BK (1998) Temporal-compositional-isotopic trends in rejuvenated-stage magmas of Kauai, Hawaii, and implications for mantle melting processes. Geochim Cosmochim Acta 62:2347–1368

Reiners PW, Nelson BK, Izuka SK (1999) Structural and petrologic evolution of the Lihue Basin and eastern Kauai, Hawaii. Geol Soc Am Bull 111:674–685

Staudigel H, Schmincke H-U (1984) The Pliocene seamount series of La Palma (Canary Islands). J Geophys Res 89:11195–11215

Vergniolle S, Mangan M (2000) Hawaiian and Strombolian eruptions. In Sigurdsson H, Houghton BF, McNutt S, Rymer H, Stix J (eds) Encyclopedia of volcanoes. Academic Press, San Diego, pp 447–461

Wohletz KH (1983) Mechanism of hydrovolcanic pyroclast formation: grain size, scanning electron microscopy, and experimental studies. J Volcanol Geotherm Res 17:31–36

Wohletz KH (2003) Water/ magma interaction: physical consideration for the deep submarine environment. In: White JD, Smellie J, Clague DA (eds) Explosive subaqueous volcanism. Am Geophys Union Monogr 140:25–49

Yang H-J, Frey FA, Clague DA (2003) Constraints on the source components of lavas forming the Hawaiian North Arch and Honolulu Volcanics. J Petrol 44:603–627

Zimanowski B, Buettner R, Lorenz V, Haefele H-G (1997) Fragmentation of basaltic melt in the course of explosive volcanism. J Geophys Res 102:803–814